scientific reports

Check for updates

OPEN

Magnetic dynamics of hedgehog in icosahedral quasicrystal

Shinji Watanabe

Quasicrystals (QCs) possess a unique lattice structure without translational invariance, which is characterized by the rotational symmetry forbidden in periodic crystals such as the 5-fold rotation. Recent discovery of the ferromagnetic (FM) long-range order in the terbium-based QC has brought about breakthrough but the magnetic structure and dynamics remain unresolved. Here, we reveal the dynamical as well as static structure of the FM hedgehog state in the icosahedral QC. The FM hedgehog is shown to be characterized by the triple-*Q* state in the reciprocal-lattice *q* space. Dynamical structure factor is shown to exhibit highly structured *q* and energy dependences. We find a unique magnetic excitation mode along the 5-fold direction exhibiting the streak fine structure in the *q* -energy plane, which is characteristic of the hedgehog in the icosahedral QC. Non-reciprocal magnetic excitations are shown to arise from the FM hedgehog order, which emerge in the vast extent of the *q* -energy plane.

Quasicrystal (QC) has a unique lattice structure with rotational symmetry forbidden in periodic crystals[1]. Although progress has been made in unraveling their atomic structure[2,3], the understanding of their electric properties remains a challenging and fascinating problem, because the Bloch theorem can no longer be applied.

The unresolved vital issue has been whether the magnetic long-range order is realized in the three-dimensional QC[4–16]. Recently, the ferromagnetic (FM) long-range order has been discovered experimentally in the QC Au-Ga-Tb[17]. Theoretically, the FM long-range order has actually been shown to be realized in the QC Au-SM-Tb (SM=Si, Al, Ge, Sn and Ga)[18,19]. Interestingly, the hedgehog state, where the magnetic moments at the Tb site located at each vertex of the icosahedron (IC) is directed outward (see Fig. 1A), has been shown to form a uniform long-range order as shown in Fig. 1B[18]. Moreover, the hedgehog state on the IC has been revealed to be characterized by the topological invariant, i.e., the topological charge of one, which exhibits emergent phenomena such as the topological Hall effect[18].

Although the FM order has been detected in the QC, the detailed magnetic structure has not been resolved experimentally[17]. Theoretically, the configurations of the magnetic moments in real space have been identified but their magnetic structure factor in reciprocal space has not been clarified[18,19]. Furthermore, the dynamical property of the magnetism in the QC remains unresolved.

As for the dynamics in the QC, the lattice dynamics was studied by inelastic X-ray and neutron scattering measurements[20,21]. The dynamical structure factor was theoretically calculated in the spin 1/2 Heisenberg model on the Fibonacci chain for the FM ground state[22] and in two-dimensional systems[23]. The dynamical structure factor was also calculated for antiferromagnetic spin 1/2 Heisenberg model on the two-dimensional octagonal tiling[24]. However, little has been known about the magnetic dynamics in the real three-dimensional QC theoretically nor experimentally.

In this report, we present the dynamical property of the uniform long-range order of the hedgehog state in the Tb-based QC. By calculating the magnetic structure factor, we show that the hedgehog is characterized as the triple-*Q* state. By analyzing the dynamical structure factor, we reveal unique energy and momentum dependences of the magnetic excitations. We find that the magnetic excitation mode along the 5-fold axis direction exhibiting streak fine structure with periodicity characterized by the wavelength of the diameter of the IC, which is considered to be characteristic of the hedgehog in the icosahedral QC. We also find the non-reciprocal magnetic excitation mode in the QC. We note that we take the unit of $\hbar = 1$ hereafter where $\hbar$ is reduced Planck constant.

Results

Lattice structure of QC. Let us start with the lattice structure of the QC. Although the FM long-range order has recently been identified by bulk measurements in the QC $Au_{65}Ga_{20}Tb_{15}$, the detailed lattice structure has not been solved experimentally[17]. In general, the rare-earth atoms in the rare-earth-based icosahedral QC

Department of Basic Sciences, Kyushu Institute of Technology, Kitakyushu, Fukuoka 804-8550, Japan. email: swata@mns.kyutech.ac.jp

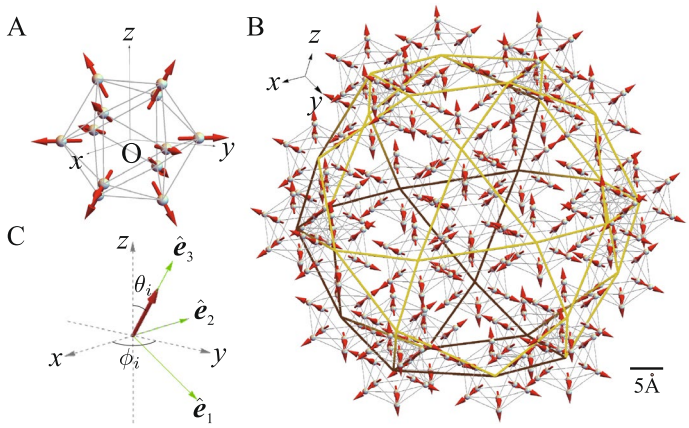

Figure 1. (**A**) The hedgehog state in the IC. Each arrow illustrates the magnetic moment at Tb, which is directed to the pseudo 5-fold axis. (**B**) The hedgehog state in $Cd_{5.7}Yb$-type QC. Green (brown) lines at the front (back) connect the vertices of the icosidodecahedron. Scale bar (5 Å) is shown in (**B**). (**C**) Local coordinate at the Tb site with the orthogonal unit vectors $\hat{\boldsymbol{e}}_1$, $\hat{\boldsymbol{e}}_2$, and $\hat{\boldsymbol{e}}_3$ (see text).

are considered to form the lattice structure of Yb in the $Cd_{5.7}Yb$-type QC[3]. Figure 1B shows the main structure of the QC where the Tb-12 cluster, i.e., IC is located at each vertex of the icosidodecahedron with the total number of the vertices being 30. In the $Cd_{5.7}Yb$-type QC, there exists a few other ICs as well as Tb sites located between the ICs. In this study, as a first step of analysis, we consider the Tb sites shown in Fig. 1B with the total lattice number $N = 12 \times 30 = 360$ to get insight into the magnetic dynamics in the QC. Here, we employ the real Tb configuration for the IC (see Fig. 1A) as well as the icosidodecahedron in the 1/1 approximant crystal (AC) $Au_{70}Si_{17}Tb_{13}$ whose lattice structure was solved by the X-ray measurement[25], as a typical case. The diameter of the IC is 10.56 Å. In Fig. 1B, the IC is located at 30 vertices of the τ^3-times enlarged icosidodecahedron in the Tsai-type cluster of $Au_{70}Si_{17}Tb_{13}$ with τ being the golden mean $\tau \equiv (1+\sqrt{5})/2$.

Minimal model in rare earth-based QC. The Tb^{3+} ion with $4f^8$ configuration has the ground state of the crystalline electric field (CEF) with the total angular momentum $J = 6$ according to the Hund's rule. The quantization axis of the CEF is the vector passing through each Tb site from the center of the IC, which is the pseudo 5-fold axis (see Fig. 1A). The detailed analysis of the CEF has revealed that the magnetic anisotropy arising from the CEF plays a key role in realizing the unique magnetic state such as the hedgehog on the IC[18,19]. Then, we consider the minimal model for the magnetism in the Tb-based QC as

$$H = \sum_{\langle i,j \rangle} J_{ij} \boldsymbol{S}_i \cdot \boldsymbol{S}_j - D \sum_i (\boldsymbol{S}_i \cdot \hat{\boldsymbol{e}}_3)^2, \tag{1}$$

where J_{ij} is the exchange interaction between the ith and jth Tb sites and $\boldsymbol{S}_i$ is the "spin" operator with $S_i = 6$. In the second term, the unit vector $\hat{\boldsymbol{e}}_3$ indicates the direction of the magnetic anisotropy arising from the CEF, which can be controlled by the compositions of Au and SM in Au-SM-Tb[18,19]. This model is expected to be relevant to not only the Tb-based QC but also rare-earth based QCs. In this study, to discuss the hedgehog state, $\hat{\boldsymbol{e}}_3$ is set to be the pseudo 5-fold axis direction. For the strong limit of the magnetic anisotropy, it has been shown that the uniform long-range order of the hedgehog state is realized in the QC for $J_2/J_1 > 2$ where $J_1(J_2)$ is the nearest neighbor (N.N.) (next N.N.) exchange interactions (Supplementary information, Fig. S1). Each IC is characterized by the topological charge of one $n_{\rm TC} = +1$, which is distributed quasi-periodically in Fig. 1B[18]. The hedgehog is the source of emergent field, which is regarded as monopole with the charge $n_{\rm TC} = +1$[26,27].

Magnetic excitation in QC. In the hedgehog state, "spins" are non-collinearly aligned as shown in Fig. 1A. Hence it is convenient to introduce the local coordinate at each Tb site where the $\hat{e}_3$ axis is set as the ordered "spin" direction as shown in Fig. 1C (see Methods section for detail). Then, by applying the Holstein-Primakoff transformation[28] to H, the "spin" operators are transformed to the boson operators as $S_i^+ = \sqrt{2S - n_i}a_i$, $S_i^- = a_i^\dagger \sqrt{2S - n_i}$ and $\boldsymbol{S}_i \cdot \hat{\boldsymbol{e}}_3^i = S - n_i$ with $n_i \equiv a_i^\dagger a_i$. Here, S_i^- (S_i^+) is the lowering (raising) "spin" operator and $a_i(a_i^\dagger)$ is an annihilation (creation) operator of the boson at the ith Tb site. Here the quadratic terms of the boson operators are retained because the higher order terms are considered to be irrelevant at least for the ground state.

We employ $J_1 = 1.0$ and $J_2 = 2.3$ as a typical parameter for the Tb-based QC. Actually, $J_2/J_1 = 2.3$ has been experimentally identified in the model Eq. (1) for the large D limit applied to the 1/1 AC $Au_{72}Al_{14}Tb_{14}$[29]. We confirmed that the hedgehog state shown in Fig. 1B with the $N = 360$ sites under open boundary condition is realized as the ground state for $D \geq 17.85$ in Eq. (1), which gives the positive excitation energy ω_i for $i = 1, \cdots, N$, as shown in Fig. 2A. The D dependence of the lowest excitation energy, i.e., the gap $\Delta \equiv \omega_N/(J_1 S)$ between the first-excited energy and the ground enegy is shown in Fig. 2B. In the spectrum, there exist several gaps, as remarkably seen in Fig. 2A as $\Delta_1 \equiv (\omega_{90} - \omega_{91})/(J_1 S)$. As D increases, the energy gap Δ as well as Δ_1

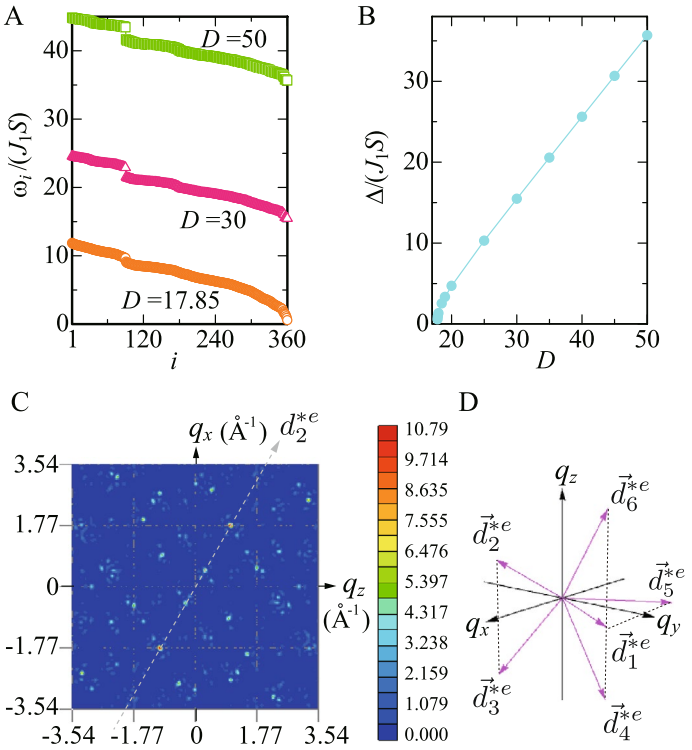

Figure 2. (**A**) ω_i vs i for $J_1 = 1.0$ and $J_2 = 2.3$ with various D. (**B**) CEF excitation gap vs D. (**C**) Top view of $F_s(\boldsymbol{q})$ in the q_z-q_x plane for $q_y = 0$. The gray dashed line in (**C**) denotes the pseudo 5-fold axis d_2^{*e} defined in (**D**). (**D**) Primitive vectors in the six-dimensional reciprocal-lattice space $\vec{d}_i^{*e}$ $(i = 1, \ldots, 6)$ as the physical (external) space components.

increases. Hereafter, we show the results for $D = 30$ as the representative case. The lowest and highest energies of the excitation spectrum are $\Delta = \omega_N/(J_1S) = 15.47$ and $\omega_1/(J_1S) = 24.59$, respectively.

Static structure factor of magnetism. Then we calculate the magnetic structure factor

$$F_s(\boldsymbol{q}) = \left\langle \left| \frac{1}{N} \sum_i \boldsymbol{S}_i e^{i\boldsymbol{q}\cdot\boldsymbol{r}_i} \right|^2 \right\rangle. \tag{2}$$

The largest peak is located at $\boldsymbol{Q}_1 \equiv (1.77, 0, 1.02)$ Å^{-1} as shown in Fig. 2C. Since the alignment of the magnetic moments in the hedgehog shown in Fig. 1A is invariant under the permutation of x, y, and z axis, the same results in $F_s(\boldsymbol{q})$ as Fig. 2C are obtained by replacing (q_x, q_y, q_z) with (q_y, q_z, q_x) and also with (q_z, q_x, q_y). Indeed we confirmed that the largest peak in $F_s(\boldsymbol{q})$ appears at $\boldsymbol{Q}_2 \equiv (0, 1.02, 1.77)$ and $\boldsymbol{Q}_3 \equiv (1.02, 1.77, 0)$ in $F_s(\boldsymbol{q})$ (Supplementary information, Figs. S2A and S2B). Namely, $F_s(\boldsymbol{Q}_1) = F_s(\boldsymbol{Q}_2) = F_s(\boldsymbol{Q}_3)$ holds. Thus the hedgehog state is characterized by the triple-Q ($\boldsymbol{Q}_1$, $\boldsymbol{Q}_2$, and $\boldsymbol{Q}_3$) state.

In Fig. 2C, the spots lie along the pseudo 5-fold axis indicated by the dashed line with an arrow named d_i^{*e}. Here, $\vec{d}_i^{*e}$ $(i = 1, \cdots, 6)$ is the primitive vector of the six-dimensional reciprocal lattice space as the physical (external) space components as shown in Fig. 2C[30]. Hereafter, we express the pseudo-5 fold axis for the $\vec{d}_i^{*e}$ direction as the d_i^{*e} line with an arrow. We note that the slope of the d_i^{*e} line for $i = 2$ in Fig. 2C is 1.736 reflecting the real configuration of the Tb sites in the IC[25] shown in Fig. 1A, which is known to be τ in the regular IC[30]. The slope of the d_3^{*e}, d_5^{*e}, and d_4^{*e} lines is the sign-reversed value of the slope of the d_2^{*e}, d_1^{*e}, and d_6^{*e} lines within each q_z-q_x, q_x-q_y, and q_y-q_z plane, respectively (see Fig. 2D).

It is noted that $S_{xx}(\boldsymbol{q})$, $S_{zz}(\boldsymbol{q})$, and $S_{yy}(\boldsymbol{q})$ have the maximum at $\boldsymbol{q} = \boldsymbol{Q}_1, \boldsymbol{Q}_2$, and $\boldsymbol{Q}_3$, respectively, where $S_{\alpha\beta}(\boldsymbol{q})$ is defined as $S_{\alpha\beta}(\boldsymbol{q}) \equiv \frac{1}{N}\sum_{i,j} e^{i\boldsymbol{q}\cdot(\boldsymbol{r}_i - \boldsymbol{r}_j)} \langle S_{i\alpha} S_{j\beta} \rangle$ $(\alpha = x, y, \text{and } z)$.

Dynamical structure factor of magnetism. The dynamical magnetic structure factor is defined as $S_{\alpha\beta}(\boldsymbol{q}, \omega) \equiv -\frac{1}{\pi}\mathrm{Im}G_{\alpha\beta}(\boldsymbol{q}, \omega)$[22], where $G_{\alpha\beta}(\boldsymbol{q}, \omega) = \frac{1}{N}\sum_{i,j} e^{i\boldsymbol{q}\cdot(\boldsymbol{r}_i - \boldsymbol{r}_j)} G_{ij}^{\alpha\beta}(\omega)$ with

$$G_{ij}^{\alpha\beta}(\omega) = \langle \mathrm{GS} | S_{i\alpha} \frac{1}{\omega + E_0 - H + i\eta} S_{j\beta} | \mathrm{GS} \rangle. \tag{3}$$

Here, $|\mathrm{GS}\rangle$ is the ground state satisfying $\alpha_i|\mathrm{GS}\rangle = 0$ and E_0 is the ground-state energy. We set $\eta = 10^{-6}$.

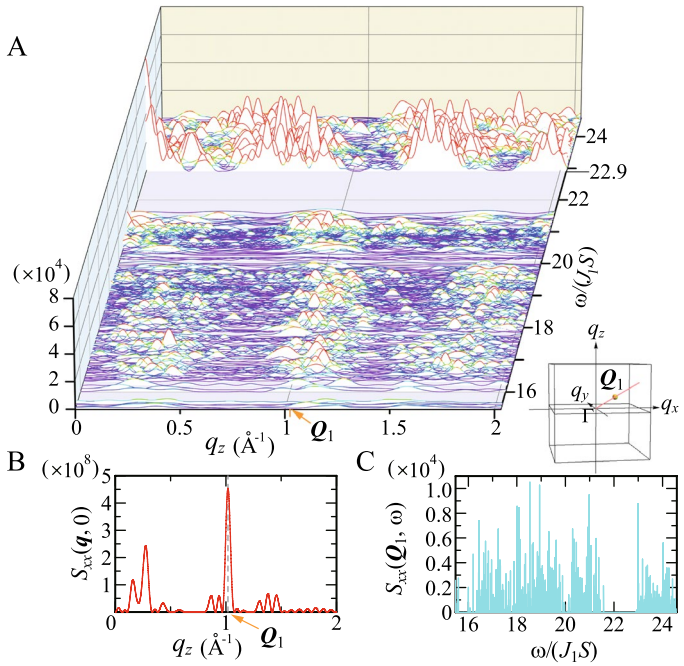

Figure 3. Dynamical structure factors (**A**) $S_{xx}(\boldsymbol{q},\omega)$ and (**B**) $S_{xx}(\boldsymbol{q},0)$ for $\boldsymbol{q}$ along the d_2^{*e} line through $\mathbf{Q}_1$ with $q_y = 0$. Inset illustrates the d_2^{*e} line through $\mathbf{Q}_1$ inside the cube with a side length of 2×3.54 Å^{-1}. (**C**) The ω dependence of $S_{xx}(\mathbf{Q}_1,\omega)$. The dashed line in (**B**) is the guide for $\boldsymbol{q} = \mathbf{Q}_1$.

The result of $S_{xx}(\boldsymbol{q},\omega)$ for $\boldsymbol{q}$ along the d_2^{*e} line in the q_z-q_x plane is shown in Fig. 3A. The spectra appear at $\omega/(J_1S) = 0$ (see Fig. 3B) with strong intensity of $\sim O(10^8)$ and also appear above the energy gap Δ with intensity of $\sim O(10^4)$. The energy gap in the excitation spectra Δ reflects the magnetic anisotropy arising from the CEF. For $\omega/(J_1S) > \Delta$, the large intensity appears at the energy $\omega_{90}/(J_1S) = 22.90$, where the highest peak appears at the Γ point. At $\omega = 0$, i.e., elastic energy, the maximum peak appears at $\boldsymbol{q} = \mathbf{Q}_1$, as shown in Fig. 3B indicated by the dashed line. In the ω dependence of $S_{xx}(\boldsymbol{q},\omega)$, spiky peak structures appear as shown in Fig. 3C for $\boldsymbol{q} = \mathbf{Q}_1$. These results indicate that the peak $S_{xx}(\mathbf{Q}_1)$ is governed by the elastic contribution $S_{xx}(\mathbf{Q}_1,0)$, which is understandable from the sum rule with respect to ω as $S_{xx}(\mathbf{Q}_1) = \frac{1}{2\pi}\int d\omega S_{xx}(\mathbf{Q}_1,\omega)$.

This is in sharp contrast to the result recently reported in the uniform long-range order of the ferrimagnetic state in the icosahedral QC[31]. Namely, the high-intensity peak appears at the ordered vector $\boldsymbol{q} = \mathbf{0}$ and the lowest CEF excitation energy $\omega/(|J_1|S) = \Delta$, from which the high-intensity peaks are continuously formed in the dynamical structure factor, giving rise to the pseudo-magnon mode[31].

Then we search the $\boldsymbol{q}$ dependence of $S_{xx}(\boldsymbol{q},\omega)$ for $\omega = \omega_{90}$ where the large intensities appear as shown in Fig. 3A. Consequently, we identify that the maximum is located at $\boldsymbol{q}_0 \equiv (2.169, 3.436, 1.442)$ Å^{-1}. Around $\boldsymbol{q} = \boldsymbol{q}_0$, we find that a series of the packet structures appears along the pseudo 5-fold axis direction, as shown in Fig. 4A where the d_2^{*e} line and d_3^{*e} line through $\boldsymbol{q} = \boldsymbol{q}_0$ is illustrated by the dashed line in the q_z-q_x plane with $q_y = 3.436$ Å^{-1}. The peak in the central packet gives the maximum $S_{xx}(\boldsymbol{q}_0,\omega_{90}) = 1.027 \times 10^5$. A series of packet structures with sub-leading intensity is also aligned along the pseudo 5-fold axis direction. For slightly larger ω than ω_{90}, the packets still appear along the d_2^{*e} line at slightly different positions as shown in Fig. 4B, which suggests the magnetic excitation propagating along the pseudo 5-fold direction.

Figure 4C shows $S_{xx}(\boldsymbol{q},\omega)$ for $\boldsymbol{q}$ along the d_2^{*e} line through $\boldsymbol{q} = \boldsymbol{q}_0$. A series of the packet structures remarkably appears at the lower edge ω_{90} with strong intensity, which continuously forms the streak with fine structure down to the lower-ω region as also seen in the intensity plot in Fig. 4D.

Interestingly, we find that a series of the packet structures is the reflection of the bottom of the continuous mode periodic along the d_2^{*e} line in the $\boldsymbol{q}$-ω plane as shown in Fig. 4D. The period of the streak structure is evaluated as $\Delta q \sim 0.6$ Å^{-1} in the reciprocal space. From the relation of the wavenumber and wavelength $\Delta q = 2\pi/\lambda$, the scale of the wavelength is estimated to be $\lambda \sim 10$ Å. It turns out that this corresponds to the diameter of the IC $d = 10.56$ Å (see Fig. 1A). Since the hedgehog is the magnetic texture on the IC, the excitation gives rise to the dynamics whose intensity decreases with periodicity $\Delta q \sim 2\pi/d$ with distance from $\boldsymbol{q}_0$ in the reciprocal space of the QC. A series of the packet structure as well as the intensity streak in the $\boldsymbol{q}$-ω plane also appears along the d_3^{*e} direction (Supplementary information, Fig. S3). The emergence of the intensity streak with fine structure in the $\boldsymbol{q}$-ω plane indicates unique excitation mode along the 5-fold axis direction, which is considered to be characteristic of the hedgehog in the icosahedral QC.

Non-reciprocal magnetic excitation in QC. To further clarify the general property of the dynamics of the hedgehog state, we show $S_{xx}(\boldsymbol{q},\omega)$ at $\omega/(J_1S) = 23.18$ for $\boldsymbol{q}$ along the pink lines in the cube whose side is parallel to the 2-fold axis $q_\alpha \in [0, 2.56]$ Å^{-1} ($\alpha = x, y,$ and z) in the inset of Fig. 5A. Here we also plot $S_{xx}(-\boldsymbol{q},\omega)$

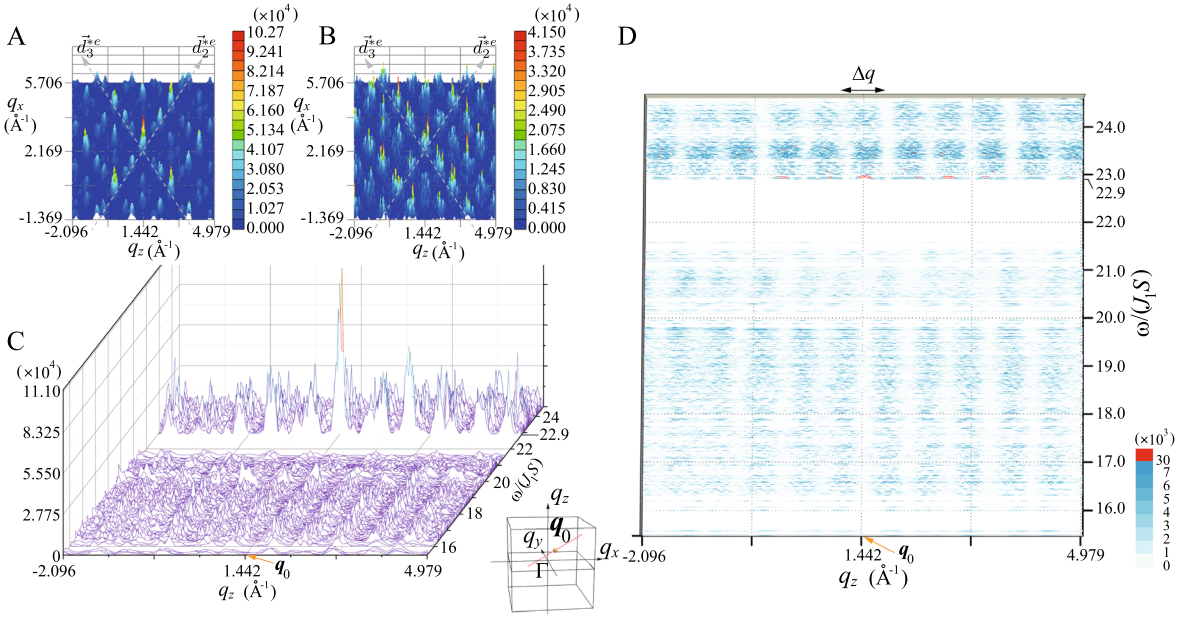

Figure 4. Dynamical structure factor $S_{xx}(\boldsymbol{q},\omega)$ in the q_z-q_x plane with $q_y = 3.436$ Å^{-1} for (**A**) $\omega/(J_1S) = 22.90$ and (**B**) 23.07. The dashed lines indicate the d_2^{*e} line and d_3^{*e} line. (**C**) $S_{xx}(\boldsymbol{q},\omega)$ for $\boldsymbol{q}$ along the d_2^{*e} line through $\boldsymbol{q}_0 = (2.169, 3.436, 1.442)$ Å^{-1}. Inset illustrates the d_2^{*e} line through $\boldsymbol{q}_0$ inside the cube with a side length of 8.31×2 Å^{-1}. (**D**) Top view of (**C**).

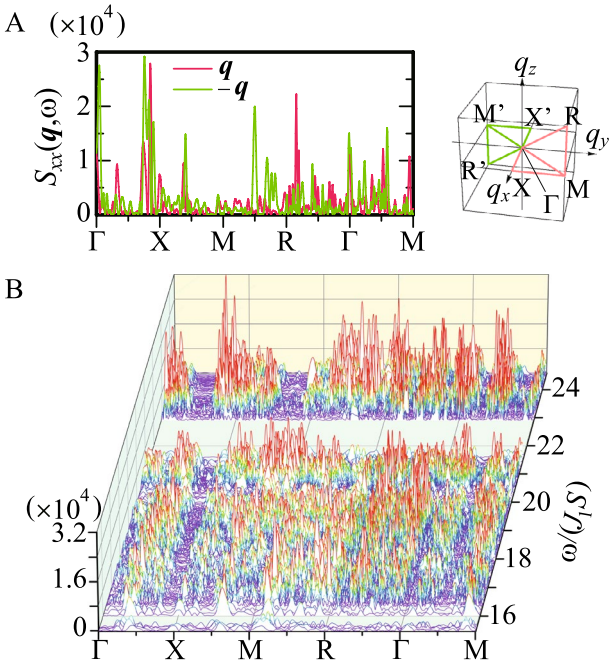

Figure 5. (**A**) Dynamical structure factor $S_{xx}(\boldsymbol{q},\omega)[S_{xx}(-\boldsymbol{q},\omega)]$ at $\omega/(J_1S) = 23.18$ for $\boldsymbol{q}$ along the pink (green) lines in the inset. Inset illustrates the cube with a side length of 2.56×2 Å^{-1}. (**B**) $|S_{xx}(\boldsymbol{q},\omega) - S_{xx}(-\boldsymbol{q},\omega)|$ for $\boldsymbol{q}$ along the pink lines in the inset and for $\omega_N \leq \omega \leq \omega_1$.

along the green line in the inset of Fig. 5A. We see remarkable differences in the intensity for $\boldsymbol{q}$ and $-\boldsymbol{q}$. In Fig. 5B, we plot $|S_{xx}(\boldsymbol{q},\omega) - S_{xx}(-\boldsymbol{q},\omega)|$ for $\boldsymbol{q}$ along the pink lines in the inset of Fig. 5A. The finite values indicate that $S_{xx}(\boldsymbol{q},\omega) \neq S_{xx}(-\boldsymbol{q},\omega)$. These results indicate that non-reciprocal magnetic excitation appears in the hedgehog state in the QC. This is, to our best knowledge, the first discovery of the non-reciprocal magnetic excitation in the topological magnetic long-range order in QC.

We confirmed that non-reciprocal magnetic excitation does not appear in the case of the collinear magnetic order in the QC (Supplementary information, Fig. S4). This implies that the noncollinear and noncoplanar

magnetic structure on the IC of the hedgehog (Fig. 1A) is the origin of the nonreciprocal excitation. Recently, non-reciprocal magnetic excitation from the uniform ferrimagnetic order (characterized by the zero topological charge $n_{\rm TC} = 0$) in the icosahedral QC has been shown to appear[31]. These results suggest that non-reciprocal excitation is common character of the noncollinear and noncoplanar alignment of the magnetic moments on the IC. As shown in Fig. 5B, emergence of many spiky peaks with fine structure as continuum are the consequence of the QC structure, which is in sharp contrast to the magnon branch in periodic crystals as the collective mode. This gives rise to the emergence of nonreciprocity as continuum in the vast extent of the $\boldsymbol{q}$-ω plane (see Fig. 5B), whose feature is unique to the QC.

Summary and discussion. We have revealed the dynamical as well as static property of the hedgehog state in the QC. The FM hedgehog state is shown to be characterized by the triple-Q state. The magnetic dynamical structure factor shows highly structured energy and momentum dependences unique to the QC. We have discovered the magnetic excitation mode along the pseudo 5-fold axis direction. A series of the packet structure in the dynamical structure factor is found to exist, which is shown to be the reflection of the periodic streak structure in the reciprocal lattice $\boldsymbol{q}$-energy ω plane. Non-collinear and non-coplanar magnetic alignment of the hedgehog state gives rise to non-reciprocal magnetic excitations which appear in the vast extent of the energy and momentum plane.

In the uniform long-range order of the ferrimagnetic state, the high-intensity peaks appear continuously from the ordered vector $\boldsymbol{q} = \boldsymbol{0}$ and the lowest CEF excitation energy $\omega = \Delta|J_1|S$, which are identified as the pseudo-magnon mode[31]. On the contrary, in the dynamical structure factor for the uniform hedgehog order, the high-intensity peaks do not appear at the ordered vector $\boldsymbol{Q}_i$ for $i = 1, 2$, and 3 beyond the CEF excitation energy. This implies that the peak in the static structure factor at the triple Q vector $\boldsymbol{q} = \boldsymbol{Q}_i$ is governed by the elastic ($\omega = 0$) contribution of the dynamical structure factor for the uniform hedgehog order.

The streak structure with periodicity characterized by the wavelength corresponding to the diameter of the IC in the $\boldsymbol{q}$-ω plane is considered to be the unique character of the excitation from the uniform hedgehog order. To establish this point, the systematic analysis of the dynamical structure factor in the magnetically ordered states in the icosahedral QC is necessary, which is left for future studies.

The non-reciprocal magnetic excitation has also been found to emerge in the uniform ferrimagnetic order[31]. Hence, as noted above, non-reciprocity is considered to be general feature of the excitation from the non-collinear and non-coplanar magnetic texture on the IC.

Our results are useful not only for resolving the magnetic structure of the long-range order discovered recently in Tb-based icosahedral QC, but also for future neutron measurements of the magnetic dynamics in the QC. So far, the dynamical structure factor in the magnetically ordered phase in the QC has not been reported. It is expected that present study stimulates future experiments to detect the dynamical property in the QC and also in the approximant crystal.

Methods

Theory of Magnetic Excitation in QC. Magnetic excitation from the uniform hedgehog long-range order in the QC can be calculated by transforming spin operators in the model (1) into boson operators. Since the hedgehog is a noncoplanar magnetic state, it is convenient to introduce the local coordinate at each Tb site[32]. The unit vectors in the global xyz coordinate $\hat{r}_1 = \hat{x}$, $\hat{r}_2 = \hat{y}$, and $\hat{r}_3 = \hat{z}$ are expressed by the local orthogonal coordinate with the unit vector $\hat{\boldsymbol{e}}_3^i$, whose direction is indicated by the polar angles (θ_i, ϕ_i), as

$$\hat{\boldsymbol{r}}_\alpha = R^i_{\alpha\beta}\hat{\boldsymbol{e}}^i_\beta \tag{4}$$

(see Fig. 1C). Here, R^i is the rotation matrix defined as

$$R^i = \begin{bmatrix} \cos\theta_i\cos\phi_i & -\sin\phi_i & \sin\theta_i\cos\phi_i \\ \cos\theta_i\sin\phi_i & \cos\phi_i & \sin\theta_i\sin\phi_i \\ -\sin\theta_i & 0 & \cos\theta_i \end{bmatrix}. \tag{5}$$

Then, the first term in Eq. (1) is expressed as

$$\sum_{\langle i,j\rangle} J_{i,j}(\boldsymbol{S}_i\cdot\boldsymbol{e}^i_\alpha)(\boldsymbol{S}_j\cdot\boldsymbol{e}^j_\beta)\sum_\gamma R^i_{\alpha,\gamma}R^j_{\gamma,\beta}. \tag{6}$$

By using $\boldsymbol{S}_i\cdot\hat{\boldsymbol{e}}^i_1 = (S^+_i + S^-_i)/2$ and $\boldsymbol{S}_i\cdot\hat{\boldsymbol{e}}^i_2 = (S^+_i - S^-_i)/(2i)$ where S^+_i and S^-_i are raising and lowering "spin" operators, respectively, we apply the Holstein-Primakoff transformation[28] to H. Namely, "spin" operators are expressed by the boson operators as $S^+_i = \sqrt{2S - n_i}a_i$, $S^-_i = a^\dagger_i\sqrt{2S - n_i}$ and $\boldsymbol{S}_i\cdot\hat{\boldsymbol{e}}^i_3 = S - n_i$ with $n_i \equiv a^\dagger_i a_i$. We retain the quadratic terms with respect to $a^\dagger_i$ and a_i, which are considered to be at least valid for the ground state. In the noncollinear magnetic state as the hedgehog, anomalous terms such as $a^\dagger_i a^\dagger_j$ and $a_i a_j$ appear. The resultant H is expressed as

$$H = [\chi^\dagger\ \tilde{\chi}]\Lambda\begin{bmatrix}\chi \\ \tilde{\chi}^\dagger\end{bmatrix}, \tag{7}$$

where $\chi^\dagger = (a^\dagger_1, a^\dagger_2, \cdots, a^\dagger_N)$ and Λ is the $2N \times 2N$ matrix. By performing the para unitary transformation

$$\begin{bmatrix} \zeta \\ \tilde{\zeta}^{\dagger} \end{bmatrix} = \mathcal{J} \begin{bmatrix} \chi \\ \tilde{\chi}^{\dagger} \end{bmatrix} \tag{8}$$

where $\zeta = (\alpha_1, \alpha_2, \cdots, \alpha_N)$ and $\mathcal{J}$ is the para unitary matrix[33], we obtain

$$H = [\zeta^{\dagger} \tilde{\zeta}] \begin{bmatrix} \bar{\omega} & \bar{0} \\ \bar{0} & \tilde{\omega} \end{bmatrix} \begin{bmatrix} \zeta \\ \tilde{\zeta}^{\dagger} \end{bmatrix}. \tag{9}$$

Here, $\bar{\omega}$ is the $N \times N$ diagonal matrix $\bar{\omega} = \mathrm{diag}(\omega_1, \omega_2, \cdots, \omega_N)$ with $\omega_i > 0, \tilde{\omega} = \mathrm{diag}(\omega_N, \omega_{N-1}, \cdots, \omega_1)$, and $\bar{0}$ is the $N \times N$ matrix with all elements being zero. Here, the index i represents the eigenvalue of the excitation energy from the magnetically ordered state.

Data availability

All the data supporting the findings are available from the corresponding author upon reasonable request.

Received: 17 June 2022; Accepted: 6 September 2022
Published online: 15 September 2022

References

1. Shechtman, D., Blech, I., Gratias, D. & Cahn, J. W. Metallic phase with long-range orientational order and no translational symmetry. *Phys. Rev. Lett.* **53**, 1951–1954 (1984).
2. Tsai, A. P., Guo, J. Q., Abe, E., Takakura, H. & Sato, T. J. A stable binary quasicrystal. *Nature* **408**, 537–538 (2000).
3. Takakura, H., Gómez, C. P., Yamamoto, A., De Boissieu, M. & Tsai, A. P. Atomic structure of the binary icosahedral Yb–Cd quasicrystal. *Nat. Mater.* **6**, 58–63 (2007).
4. Hattori, Y. *et al.* Spin-glass behaviour of icosahedral Mg–Gd–Zn and Mg–Tb–Zn quasi-crystals. *J. Phys. Condens. Matter* **7**, 2313 (1995).
5. Hattori, Y. *et al.* Electronic specific heat coefficient and magnetic entropy of icosahedral Mg–RE–Zn (RE=Gd, Tb and Y) quasicrystals. *J. Phys. Condens. Matter* **7**, 4183 (1995).
6. Charrier, B. & Schmitt, D. Dynamical and irreversible magnetic effects in i-$R_8Mg_{42}Zn_{50}$ quasicrystals (R=Tb, Dy). *J. Magn. Magn. Mater.* **171**, 106 (1998).
7. Islam, Z. *et al.* Reinvestigation of long-range magnetic ordering in icosahedral Tb–Mg–Zn. *Phys. Rev. B* **57**, R11047 (1998).
8. Sato, T. J., Takakura, H., Tsai, A. P. & Shibata, K. Anisotropic spin correlations in the Zn–Mg–Ho icosahedral quasicrystal. *Phys. Rev. Lett.* **81**, 2364 (1998).
9. Fisher, I. R. *et al.* Magnetic and transport properties of single-grain R–Mg–Zn icosahedral quasicrystals [R=Y, $(Y_{1-x}Gd_x)$, $(Y_{1-x}Tb_x)$, Tb, Dy, Ho, and Er]. *Phys. Rev. B* **59**, 308 (1999).
10. Sato, T. J. *et al.* Antiferromagnetic spin correlations in the Zn–Mg–Ho icosahedral quasicrystal. *Phys. Rev. B* **61**, 476 (2000).
11. Dolinšek, J., Jagličić, Z., Chernikov, M. A., Fisher, I. R. & Canfield, P. C. Unusual spin-glass phase in icosahedral Tb–Mg–Zn quasicrystals. *Phys. Rev. B* **64**, 224209 (2001).
12. Sato, T. J., Guo, J. & Tsai, A. P. Magnetic properties of the icosahedral Cd-Mg-rare-earth quasicrystals. *J. Phys. Condens. Matter* **13**, L105 (2001).
13. Sato, T. J., Takakura, H., Guo, J., Tsai, A. P. & Ohoyama, K. Magnetic correlations in the Cd–Mg–Tb icosahedral quasicrystal. *J. Alloys Compd.* **342**, 365 (2002).
14. Sebastian, S. E., Huie, T., Fisher, I. R., Dennis, K. W. & Kramer, M. J. Magnetic properties of single grain R–Mg–Cd primitive icosahedral quasicrystals (R= Y, Gd, Tb or Dy). *Philos. Mag.* **84**, 1029 (2004).
15. Goldman, A. I. *et al.* A family of binary magnetic icosahedral quasicrystals based on rare earths and cadmium. *Nat. Mater.* **12**, 714 (2013).
16. Suzuki, S. *et al.* Magnetism of Tsai-type quasicrystal approximants. *Mater. Trans.* **62**, 298–306 (2021).
17. Tamura, R. *et al.* Experimental observation of long-range magnetic order in icosahedral quasicrystals. *J. Am. Chem. Soc.* **143**(47), 19938 (2021).
18. Watanabe, S. Magnetism and topology in Tb-based icosahedral quasicrystal. *Sci. Rep.* **11**, 17679 (2021).
19. Watanabe, S. Topological magnetic textures and long-range orders in Terbium-based quasicrystal and approximant. *Proc. Natl. Acad. Sci. USA* **118**(43), e2112202118 (2021).
20. Quilichini, M. & Janssen, T. Phonon excitations in quasicrystals. *Rev. Mod. Phys.* **69**, 277 (1997).
21. de Boissieu, M. *et al.* Lattice dynamics of the Zn–Mg–Sc icosahedral quasicrystal and its Zn-Sc periodic 1/1 approximant. *Nat. Mater.* **6**, 977 (2007).
22. Ashraff, J. A. & Stinchcombe, R. B. Dynamic structure factor for the Fibonacci-chain quasicrystal. *Phys. Rev. B* **39**, 2670 (1989).
23. Ashraff, J. A., Luck, J. M. & Stinchcombe, R. B. Dynamic structure factor for the Fibonacci-chain quasicrystal. *Phys. Rev. B* **41**, 4314 (1990).
24. Wessel, S. & Milat, I. Quantum fluctuations and excitations in antiferromagnetic quasicrystals. *Phys. Rev. B* **71**, 104427 (2005).
25. Hiroto, T. *et al.* Noncoplanar ferrimagnetism and local crystalline-electric-field anisotropy in the quasicrystal approximant $Au_{70}Si_{17}Tb_{13}$. *J. Phys. Condens. Matter* **32**, 415802 (2020).
26. Kanazawa, N. *et al.* Critical phenomena of emergent magnetic monopoles in a chiral magnet. *Nat. Commun.* **7**, 11622 (2016).
27. Tokura, Y. & Kanazawa, N. Magnetic skyrmion materials. *Chem. Rev.* **121**, 2857 (2021).
28. Holstein, T. & Primakoff, H. Field dependence of the intrinsic domain magnetization of a ferromagnet. *Phys. Rev.* **58**, 1098 (1940).
29. Sato, T. J. *et al.* Whirling spin order in the quasicrystal approximant $Au_{72}Al_{14}Tb_{14}$. *Phys. Rev. B* **100**, 054417 (2019).
30. Yamamoto, A. Crystallography of quasiperiodic crystals. *Acta Cryst.* **A52**, 509 (1996).
31. Watanabe, S. Magnetic dynamics of ferromagnetic long range order in icosahedral quasicrystal. *Sci. Rep.* **12**, 10792 (2022).
32. Haraldsen, J. T. & Fishman, R. S. Spin rotation technique for non-collinear magnetic systems: application to the generalized Villain model. *J. Phys. Condens. Matter* **21**, 216001 (2009).
33. Colpa, J. H. P. Diagonalization of the quadratic boson hamiltonian. *Phys. A* **93**, 327 (1978).

Acknowledgements

The author thanks M. Matsuura and T. Ishimasa for valuable discussion. This work was supported by JSPS KAKENHI Grant Numbers JP18K03542, JP19H00648, JP22H0459, and JP22H01170.

Author contributions

S.W. conceived the study and led the project. Theoretical calculation was performed by S.W. The manuscript was written by S.W.

Competing interests

The author declares no competing interests.

Additional information

Supplementary Information The online version contains supplementary material available at https://doi.org/10.1038/s41598-022-19870-6.

Correspondence and requests for materials should be addressed to S.W.

Reprints and permissions information is available at www.nature.com/reprints.

Publisher's note Springer Nature remains neutral with regard to jurisdictional claims in published maps and institutional affiliations.